Submitted: 18 April, 2023 Accepted: 04 July, 2023 Published: 03 January, 2024 DOI:10.22514/jocpd.2024.019

ORIGINAL RESEARCH

Journal of Clinical Pediatric Dentistry

Arm design of band and loop space maintainer affects its longevity: a patient-specific finite element study

Özgür Doğan[1,*], Suat Serhan Altıntepe Doğan[2]

[1]Department of Pediatric Dentistry, Faculty of Dentistry, University of Afyonkarahisar Health Science, 03040 Afyonkarahisar, Turkey
[2]Department of Periodontology, Faculty of Dentistry, University of Afyonkarahisar Health Science, 03040 Afyonkarahisar, Turkey

***Correspondence**
ozgurdogan1984@gmail.com
(Özgür Doğan)

Abstract

Fixed space maintainers (FSMs) are commonly utilized in pediatric dentistry to prevent space loss following premature tooth extraction. Although previous studies have examined the survival rates and causes of FSM failure, the impact of arm design on failure has not been investigated. This study aimed to investigate the tensile and compressive stresses related to FSMs with different arm designs and evaluate the effect of arm designs on FSM failure. Cone beam computed tomography images of a child who experienced premature loss of a primary mandibular left second molar tooth were retrieved from our database, then processed and simulated using the Rhinoceros software. Finite element analysis was performed to evaluate the stresses on four distinct FSM arm designs under simulated chewing forces. The results showed that the straight-arm FSM design exhibited the highest von Mises principal stress, while FSMs with curved arms and surrounding primary mandibular left first molar in the mesial area demonstrated the lowest von Mises stress accumulation. Intense stress accumulation on the distal surface of tooth 74 was observed in the test models due to the transmitted forces by the FSM. The maximum principal stresses accumulated at the base of the alveolar socket of the mesial root of tooth 36, while the minimum principal stresses were identified at the mesio-marginal area of the alveolar crest. The arm design played a crucial role in enabling the appliance to effectively withstand the stresses accumulating on the Space maintainer (SM) and orthodontic band. Bending the SM arms to match the surrounding profile with curvature increased the stress absorption capacity by increasing the arm length.

Keywords

Fixed space maintainer; Finite element analysis; Primary molar; Band and loop; Tooth loss

1. Introduction

Fixed space maintainers (FSMs) are used in dentistry to preserve edentulous spaces resulting from elective tooth extraction or premature tooth loss [1, 2]. Pediatric dentists play a vital role in safeguarding these spaces during the transitional period before the eruption of permanent teeth [3].

Loss of space following early extraction of primary molars commonly occurs in both primary and mixed dentition unless an FSM is used [4]. Space maintainer (SM) placement can effectively prevent undesirable tooth movements that might have otherwise caused malocclusions, such as mesial drifting or tipping [5]. The most common cause of malocclusions is reduced dental arch length due to premature loss of primary teeth [1]. Therefore, immediate measures should be taken following the early extraction of primary second molars to prevent both space loss and reduction in arch length [3], and when choosing an appropriate SM for the edentulous site, pediatric dentists should consider factors such as the stage of dental development, dental arch and the number of teeth lost [6]. Among the various types of SMs available, the band and loop (B&L) SM is the most commonly preferred option in pediatric dentistry [3].

Finite element analysis (FEA) was originally developed in the field of engineering to study stress patterns in complex structures, allowing for the examination of stress distribution within different components of the structure. FEA involves the conversion of the site in which stresses accumulate into a mesh consisting of elements and nodes [7]. This computer-dependent numerical analysis is the most common method of calculating complex conditions of stress distribution encountered in dental systems [8].

SM failure has been attributed to decementation and band and solder breakage [9, 10]. However, there is a lack of studies examining the impact of SM arm design on stress accumulation. This study aimed to assess the stresses experienced by SM bands and arms using FEA, providing novel insights into this area of research.

The hypothesis of this study postulated that the design of

the SM arms may not significantly impact the accumulation of stress on both the SM band and arms.

2. Materials and methods

The present study made use of clinical scenario simulation to evaluate four distinct arm designs of FSM. To obtain accurate results in FEA, the study models were made to simulate clinical conditions with absolute accuracy. For this study, a Turkish female patient was chosen from our research hospital's cone beam computerized tomography (CBCT) database. Then, a three-dimensional (3D) geometric model was constructed using CBCT volumetric data of the orofacial region of an eight-year-old girl with a section thickness of 0.2 mm. The Digital Imaging and Communications in Medicine (DICOM) data were then exported to the 3D Doctor Software (version 4.0, Able Software Corp., Lexington, MA, USA) in the Digital Imaging Communications in Medicine 3.0 format for segmentation. The cancellous and cortical bone was segmented based on Hounsfield units using an interactive segmentation method in the 3D Doctor software. Afterward, the geometric data were manually revised and corrected to smoothen the model and fill in any gaps left by the automated segmentation. The resulting 3D models were further processed using the 3D complex rendering method and saved as stereolithography (.stl) files. The surface geometries of Tooth-bone-Space Maintainer (TB-SM) consisted of enamel, dentin, alveolar bone and the roots with gingiva and root canal. Specifically, the TB-SM model included a primary mandibular first molar treated with pulpotomy and fitted with a stainless steel crown (tooth number 74) and a permanent mandibular first molar (tooth number 36) (Fig. 1). The 3D spatial coordinates of all models were imported and assembled in the Rhinoceros 4.0 software (3670 Woodland Park Ave N, Seattle, WA 98103 USA), following which the cortical, cancellous bones, teeth and periodontal ligament (PDL) were reconstructed based on their anatomical dimensions. Additionally, four patterns of SM arms were created using the Rhinoceros software. The PDL was modeled as a 0.2 mm thickness using a boolean operation, and an orthodontic band was designed to surround the crown of tooth number 36 (Fig. 1).

A 3D mesh capturing the dimensional and topographic details of the enamel and dentin structures, along with different B&L SMs and arm designs, was created using VRMesh Studio (VirtualGrid Inc., Bellevue, WA, USA) [11, 12]. The 3D FEA was performed using the subject-specific geometry of the TB-SM. Then, study models with uniform thickness were constructed to fit the TB-SM. The 3D geometry of the TB-SM was constructed by generating an element mesh using the quadratic tetrahedron type through a surface modeling approach in the meshing process. This approach aimed to achieve a more detailed and realistic 3D model. Convergence analysis was performed on the models to refine mesh quality. Based on the mesh convergence analysis (h-adaptivity), all models reached convergence when the inter-analysis stress variation was less than 3%. The total number of nodes and elements decreased on average by 162.944 and 735.096, respectively, with a calculated maximum error of 0.90%. The element size for quality was 0.1 mm, especially between the SM-TB-PDL complex. This modeling technique created a high-quality mesh structure with a maximum number of nodal elements for stress analyses [13]. In addition, we used an adaptive meshing option to preserve the thin and fine structures of enamel and dentin structures. The surface-refined five tooth-bone-SM complex (TB-SM) was then transferred to the Algor Fempro (version 23.0, ALGOR, Inc. 150 Beta Drive Pittsburgh, PA 15238-2932, USA) software for FEA by maintaining the model's 3D coordinates (Fig. 1) [11].

Young's modulus and Poisson's ratios were used to define the material physical properties of the TB-SM components, and the behavior of all dental tissues and materials was incorporated into the models. The material properties were set in the Algor Fempro software. All dental tissues and materials were assumed to be homogenous, isotropic and linearly elastic (Fig. 1).

Table 1 displays the values obtained from a previous FEA, including the results of static FEA with and without four patterns of SMs. Additionally, the table provides information about the number of nodes and elements used in the meshing process for all models.

2.1 Model generation

Control Model: This model represents a scenario where the chewing force is applied without using a space maintainer after a premature tooth extraction (Fig. 2A,B).

Test Model One: This model represents a scenario where an FSM with straight arms was positioned in the area of the premature tooth extraction (Fig. 3A–C). In this model, the angle between the space maintainer and tooth 74 is 33.46° for the small angle and 146.53° for the large angle.

Test Model Two: This model represents a scenario where a space maintainer with straight arms surrounds tooth 74 (Fig. 4A–C). The angle between the space maintainer and tooth 74 is 33.46° for the small angle and 146.53° for the large angle.

Test Model Three: This model represents a scenario where an FSM with curved arms was placed (Fig. 5A–E). The curvature angles of the space maintainer arms are 154.9° for the larger angle and 25.05° for the smaller angle. Additionally, the angle between the space maintainer and tooth 74 is 33.46° for the small angle and 146.53° for the large angle.

Test Model Four: This model represents a scenario in which an FSM with curved arms surrounded tooth 74 (Fig. 6A–E). The curvature angles of the space maintainer arms are 151.95° for the larger angle and 28.04° for the smaller angle. Furthermore, the angle between the space maintainer and tooth 74 is 75.04° for the small angle and 104.95° for the large angle.

2.2 Boundary conditions

In the FEA, the boundary conditions were set as follows: a fixed condition was applied to the coronal, sagittal and transverse planes of the mandible; the out-of-plane constraint condition was set at the cutting plane of the SM; all interfaces, such as the cortical and cancellous bone and cortical bone-PDL, were continuous and inseparable, while teeth and PDL were modeled using a bonded contact algorithm, which only allows small sliding movements. In the TB-SM complex,

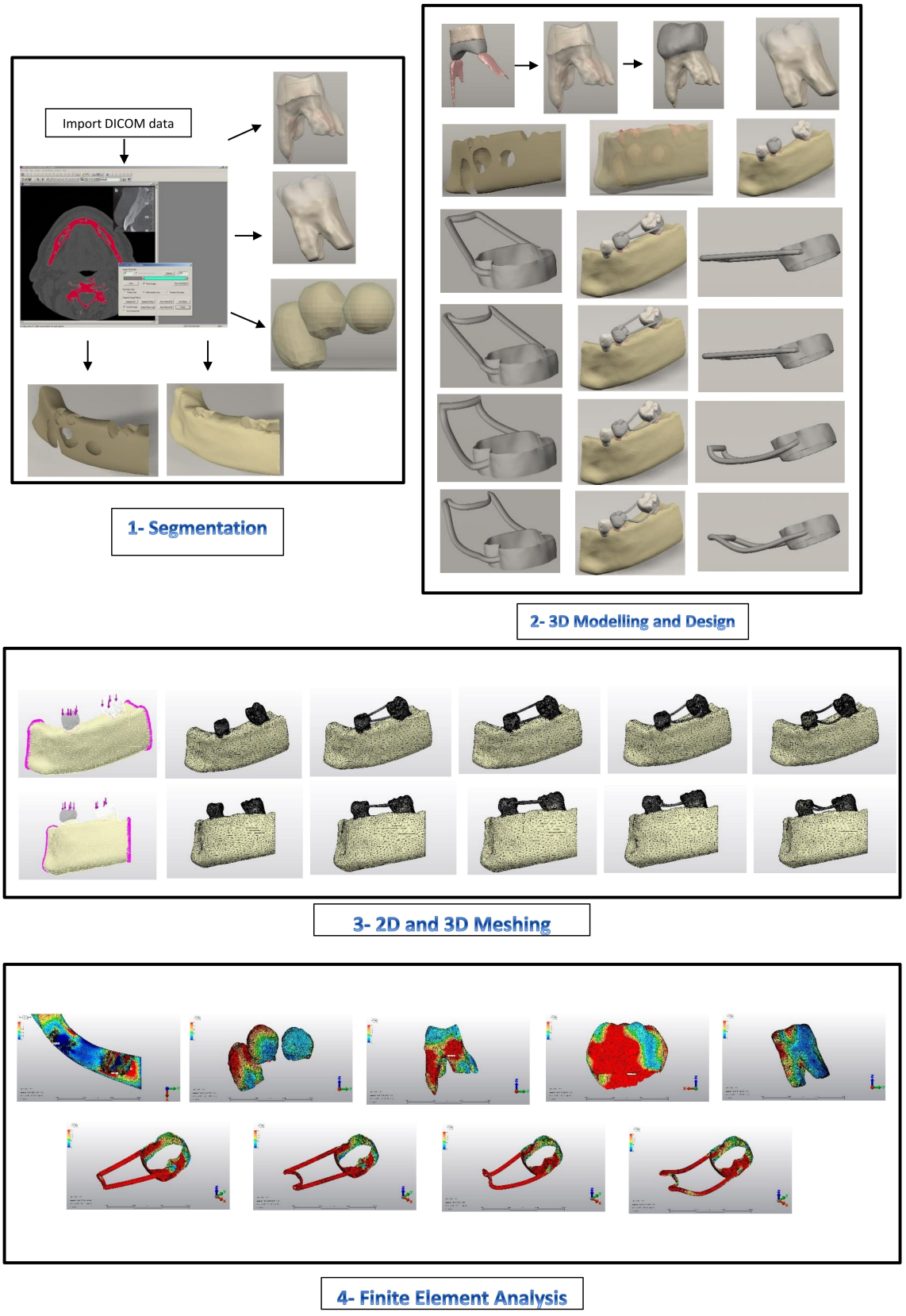

FIGURE 1. Flow chart depicting the generation of the model. In stage 1, the CBCT dataset was imported to 3D Doctor Software for segmentation of teeth, cortical and cancellous bones. Stage 2 involved assembling teeth with pulps, cortical and cancellous bones, and fixed space maintainers using the Rhinoceros Software. In Stage 3, the assembled study models were exported from Rhinoceros Software to VRMesh for meshing and generating simulation models using VRMesh Studio. In the final stage, stress analyses on all models were performed using the Algor Fempro Software.

TABLE 1. Young modulus and Poisson ratios of dental structures and other materials.

Structure	Young Modulus (Mpa)	Poisson Ratios
Enamel	41,000	0.30 [14]
Dentin	18,600	0.31 [14]
Periodontal Ligament	50	0.49 [15]
Cortical Bone	13,700	0.30 [14]
Cancellous Bone	1400	0.30 [14]
Stainless Steel	210,000	0.30 [16]
Glass Ionomer Cement	12,000	0.25 [17]

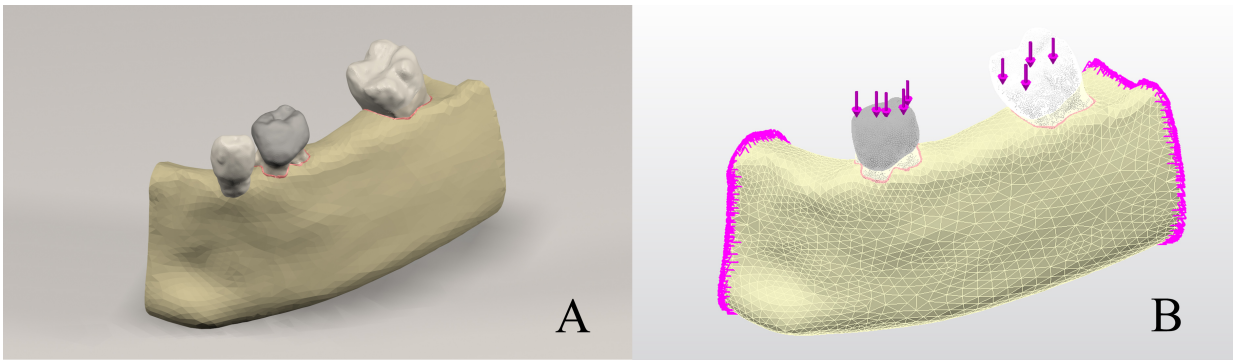

FIGURE 2. Generation of the control model. (A) Model generation based on CBCT scan. (B) Bone cutting surface of the mandible and boundary condition, with a load of 289.28 N applied on 4 points in the axial direction.

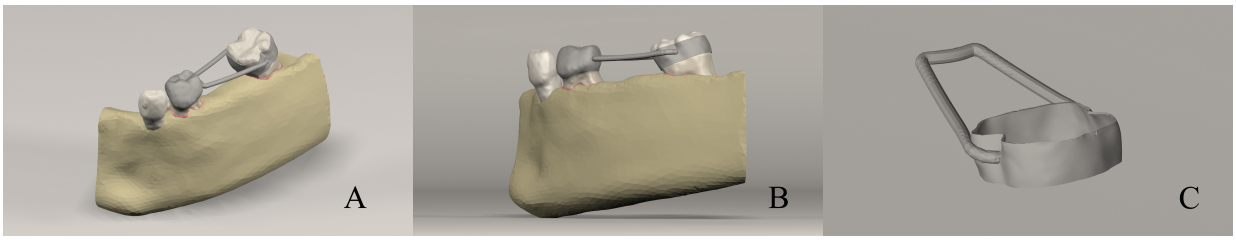

FIGURE 3. Generated 3D simulation model of test model 1. (A) FSM with straight arm type. (B) Sagittal view of straight arm FSM. (C) Render Image of Test Model 1.

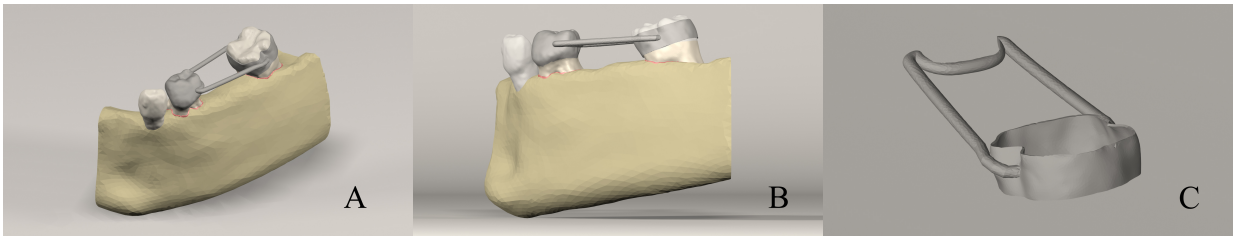

FIGURE 4. Generated 3D simulation model of test model 2. (A) FSM with straight and surround-type arms. (B) Sagittal view of FSM. (C) Render Image of Test Model 2.

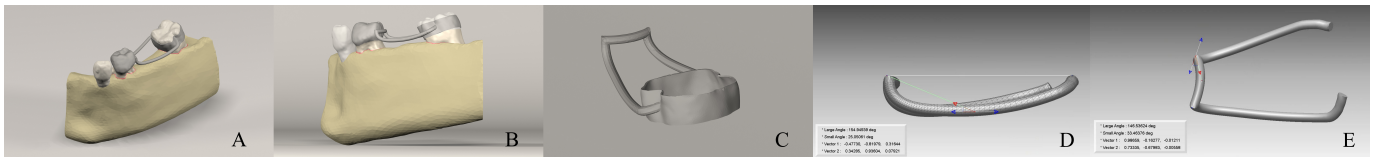

FIGURE 5. Generated 3D simulation model of test model 3. (A) Curved arm type of FSM. (B) Sagittal view of FSM. (C) Render Image of Test Model 3. (D) Sagittal view of the angles of the curved arm type of FSM. (E) Horizontal view of the angles of the curved arm type of FSM.

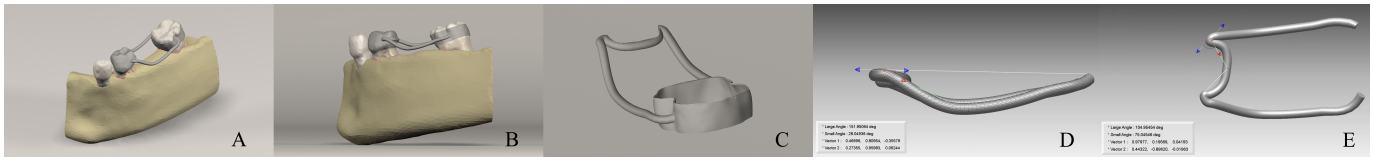

FIGURE 6. Generated 3D simulation model of test model 4. (A) Curved and surround-type arms of FSM. (B) Sagittal view of FSM. (C) Render Image of Test Model 4. (D) Sagittal view of the angles of the curved and surround arm type of FSM. (E) Horizontal view of the angles of the curved and surround arm type of FSM.

the displacement field between TB, SM and SM-cement layer (0.02 mm) contacts was applied bonded [14]. A friction coefficient of 0.2 was assigned between the tooth and SM [18, 19]. A surface-to-surface contact condition was applied to represent the connection between the SM and tooth-bone (TB) complex. However, during the application of the chewing force, a nodal separation of the SM from the tooth complex was allowed.

2.3 Simulation of force loading and FEA

As shown in Fig. 1, a static loading condition of a 289.28 N chewing force was applied to teeth 74 and 36 on the occlusal surface in a vertical direction along their long axis for one second, as described in previous studies [12, 20, 21]. For the chewing force loading simulation, the total force of 289.28 N was evenly distributed across five different functional contact points (Fig. 2A). While the loading area would be extremely small in a real clinical situation, using a point loading condition is a reasonable approximation to examine the overall stress distribution in the TB-SM complex. To analyze the stress distribution, a stress analysis was performed using the Algor Fempro software [11].

2.4 Statistical analyses and interpretation of analysis results

The one-way analysis of variance (ANOVA) test was used to assess the differences between different groups of a qualitative variable concerning a quantitative variable, considering the presence of assumptions regarding mean distribution. Then, the Tukey *post hoc* test was used for pairwise comparisons of significant differences in the one-way ANOVA test. The statistical significance level was set as 0.05.

Stress values in the SM band and arms were calculated using the von Mises stresses. The highest maximum and minimum principal stresses of cortical and cancellous bones were calculated. The maximum and minimum principal stresses of the cortical and cancellous bones were determined. Additionally, the maximum and minimum principal stresses and von Mises stress values were recorded on the lingual and buccal arms of the FSM. A linear color scale was employed to visualize both types of stress. Areas with the highest stress concentration were represented in red for von Mises and maximum principal stresses, while areas with the lowest values of the minimum principal stresses were shown in blue. Furthermore, the principal stress values were examined, with positive values indicating tensile stresses (maximum principal) and negative values indicating compressive stresses (minimum principal).

3. Results

When the simulation models were compared, the statistical analysis revealed significant differences in the von Mises stresses on the buccal and lingual arms among the four test groups ($p < 0.001$). The Tukey *post hoc* test further demonstrated significant differences between all paired groups for the buccal arms ($p < 0.05$). The highest von Mises stresses were observed on the buccal arms in Test Model One (Figs. 7,8), followed by Test Models Two (Figs. 7,9), Four (Figs. 7,11), and Three (Figs. 7,10), respectively. On the other hand, the von Mises stresses on the lingual arms were highest in Test Model Two (Figs. 7,9), followed by Test Models Four (Figs. 7,11), Three (Figs. 7,10), and One (Figs. 7,8), respectively ($p < 0.001$).

When analyzing the orthodontic bands independently, it was observed that the von Mises stresses accumulated more on the buccal surface of the band compared to its lingual surface in all test groups (Fig. 12). The highest von Mises stresses were found on the mesial surface of the orthodontic bands (Figs. 8,9). Significant differences were identified in the orthodontic band surface stress levels among the four groups ($p < 0.001$). The highest stresses were observed in Test Model One (Fig. 8), followed by Test Models Three (Fig. 10), Two (Fig. 9) and Four (Fig. 11), respectively. Multiple comparisons and test models also revealed significant differences ($p < 0.001$, ($p = 0.012$ for Test Model Two and Three comparisons)). Further, relatively lower von Mises stresses were found to accumulate on the distal surfaces and gingival portions of the orthodontic bands in all study groups (Figs. 8,9,10,11).

The analysis revealed that the von Mises stresses were higher in the lingual arms than the buccal arms in all study groups (Figs. 7,8,9,10,11). This trend was also observed in the accumulation of von Mises stresses on the orthodontic bands. Additionally, the contact point with tooth 74 was identified as the site of von Mises stress accumulation in all study groups (Fig. 13). We also observed significant differences ($p < 0.001$) in the distolingual and distobuccal contacts among the four groups, with multiple comparisons and test models further confirming the significant differences ($p < 0.001$). Further, significant differences were also found between all paired groups within the four different groups ($p < 0.001$).

The von Mises stresses resulting from chewing forces predominantly accumulated on the distal surface of stainless steel crowns and their roots in tooth 74 (Fig. 14). In comparison to the control model, the test models exhibited a pronounced stress accumulation on the distal surface of tooth 74 (Fig. 14). In addition, we observed a significant difference in the von Mises stress on the distal surface of tooth 74 across the five

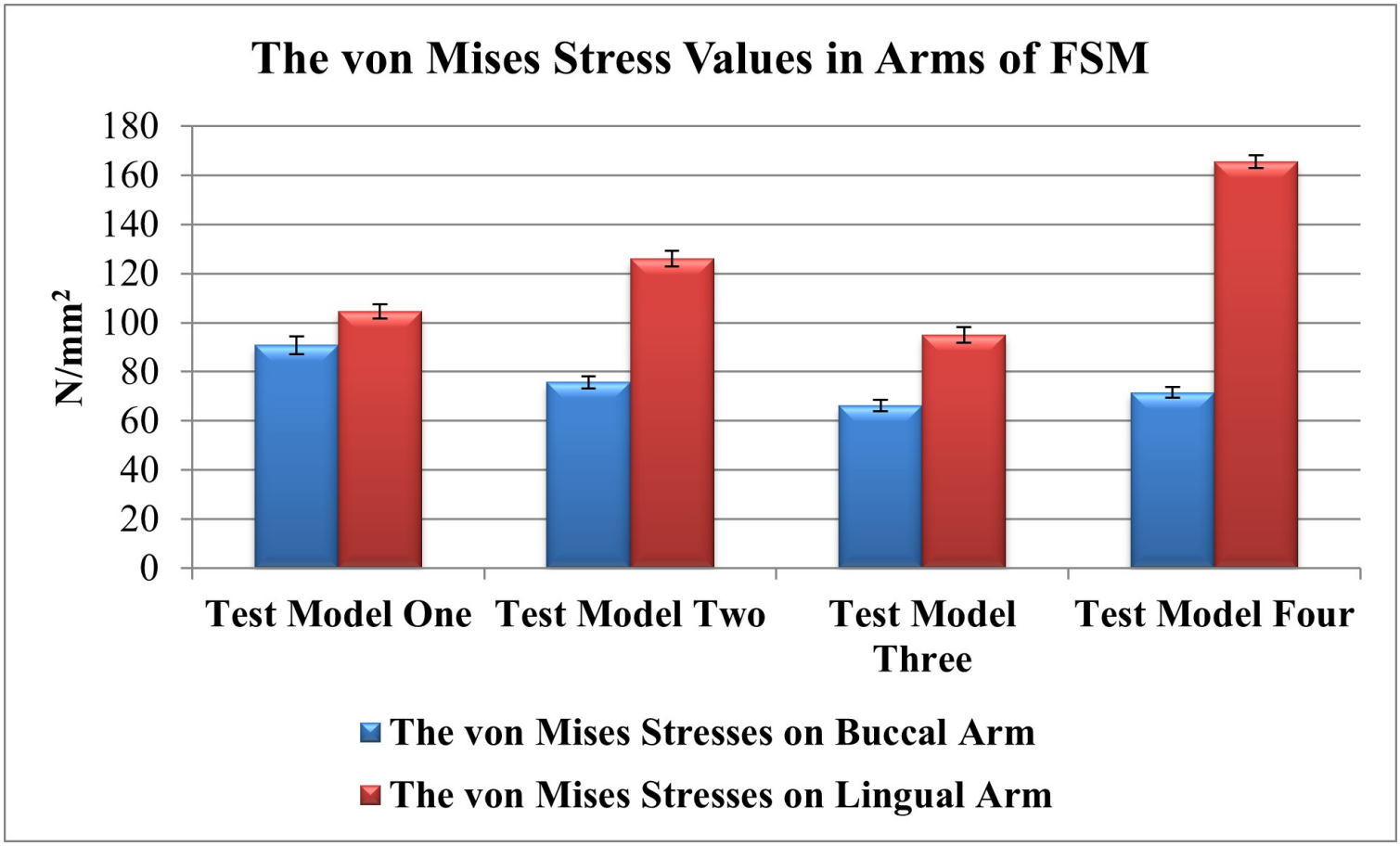

FIGURE 7. The von Mises Stress values in the FSM arms of all test models. FSM: Fixed space maintainer.

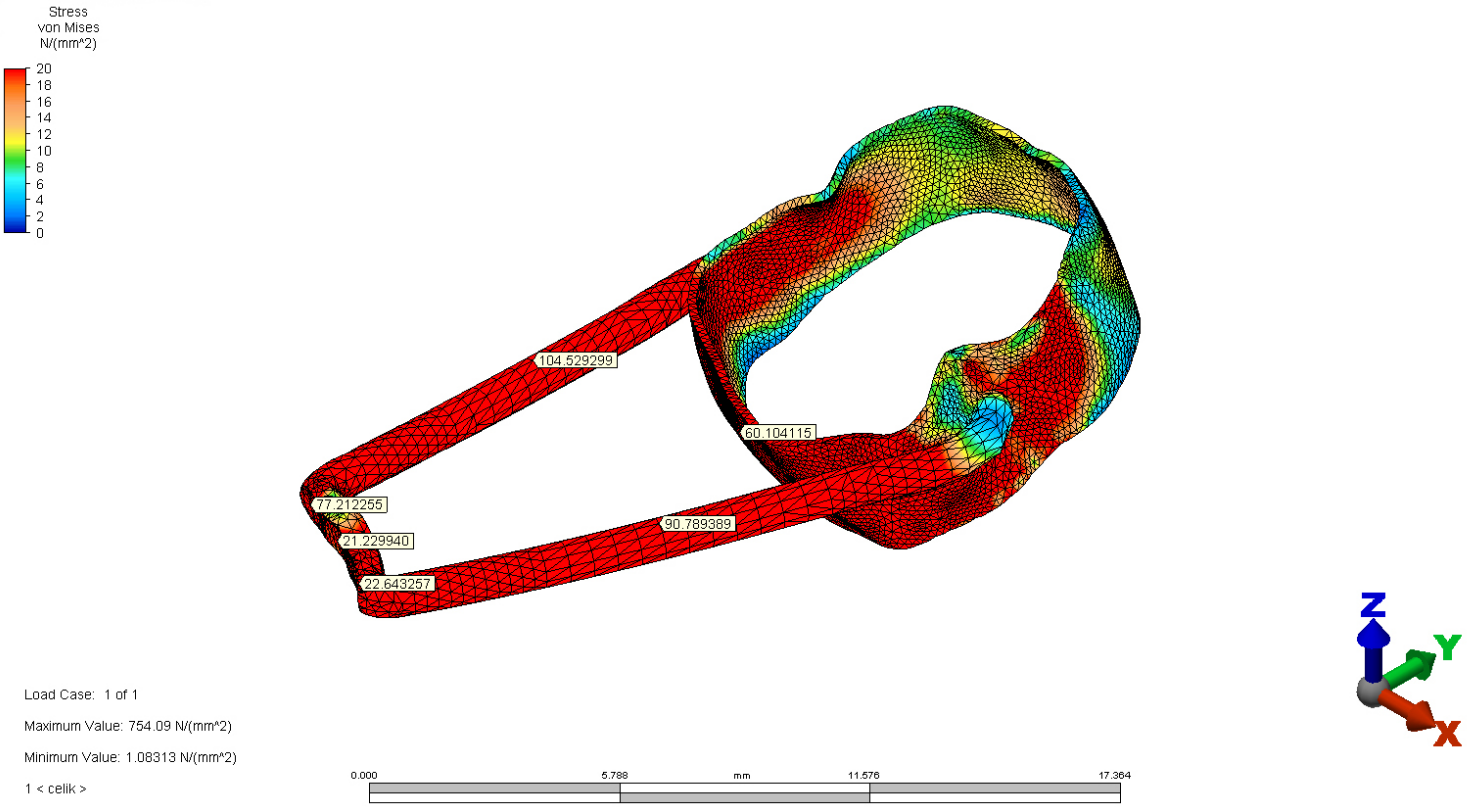

FIGURE 8. FSM with straight arms. The von Mises Stress Scale of the Control Group in Test Model 1 is shown using a stress scale and spatial coordinates.

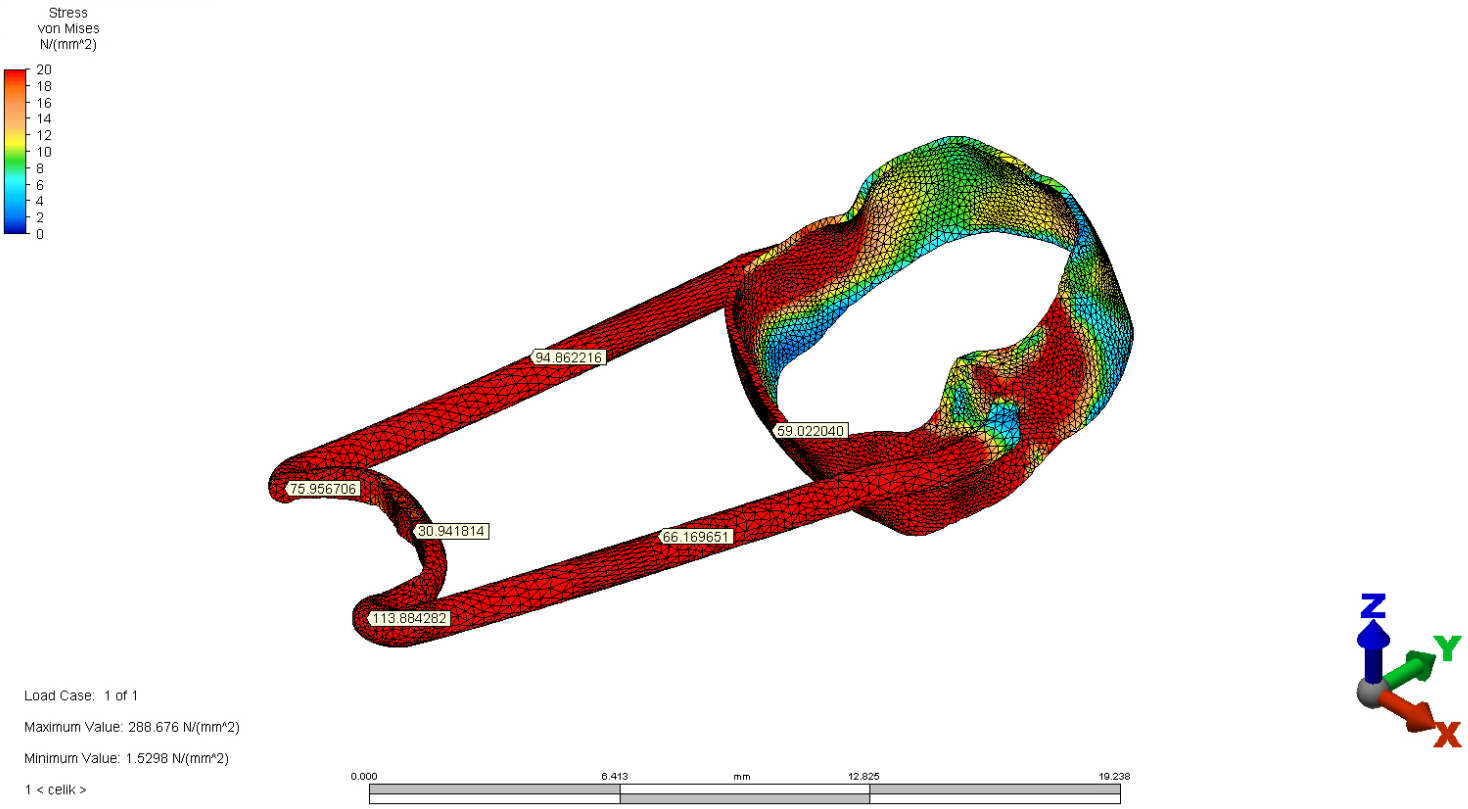

FIGURE 9. FSM with straight and surround arms. The von Mises Stress Scale in Test Model 2 is shown using a stress scale and spatial coordinates.

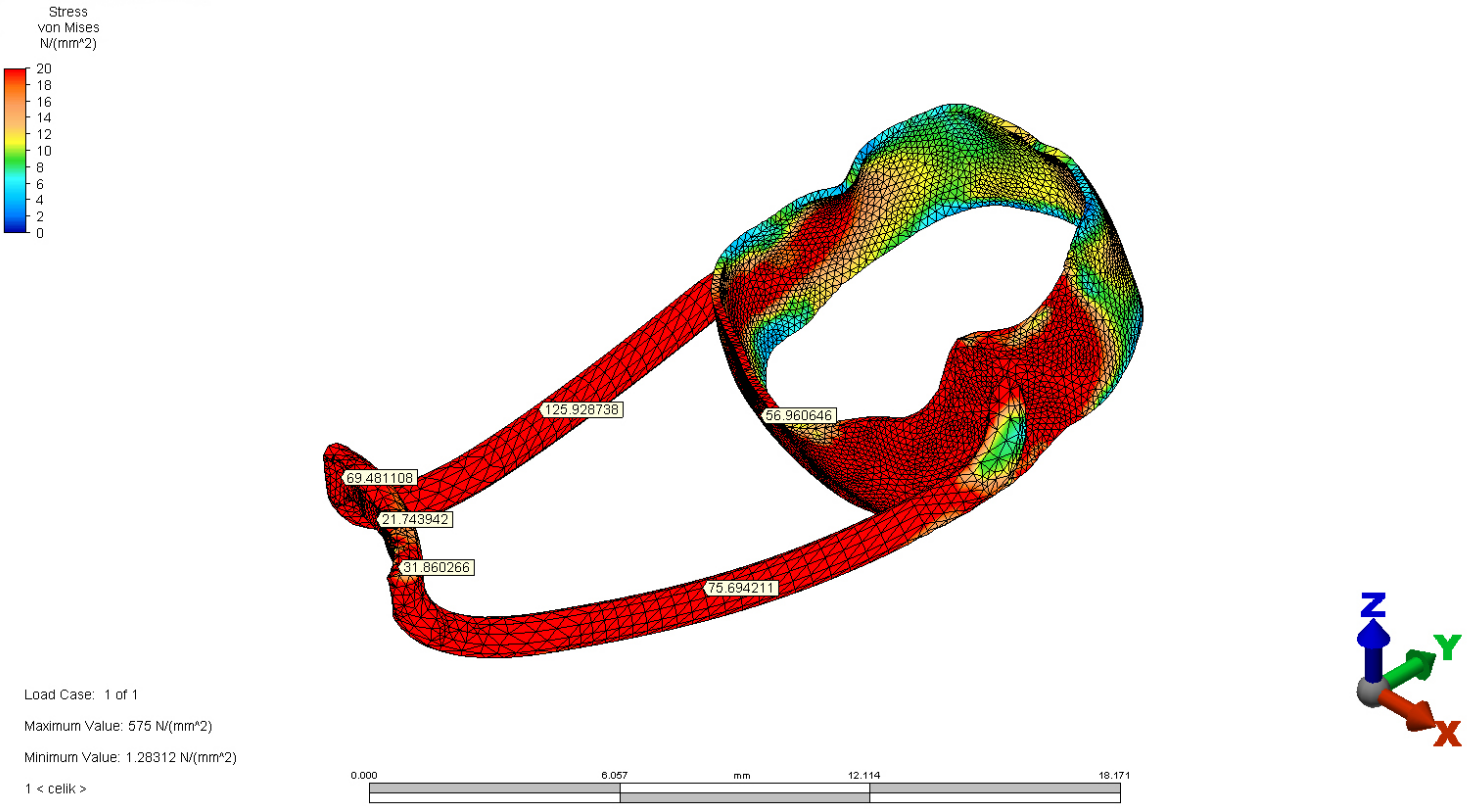

FIGURE 10. FSM with curved arms. The von Mises Stress Scale in Test Model 3 is shown using a stress scale and spatial coordinates.

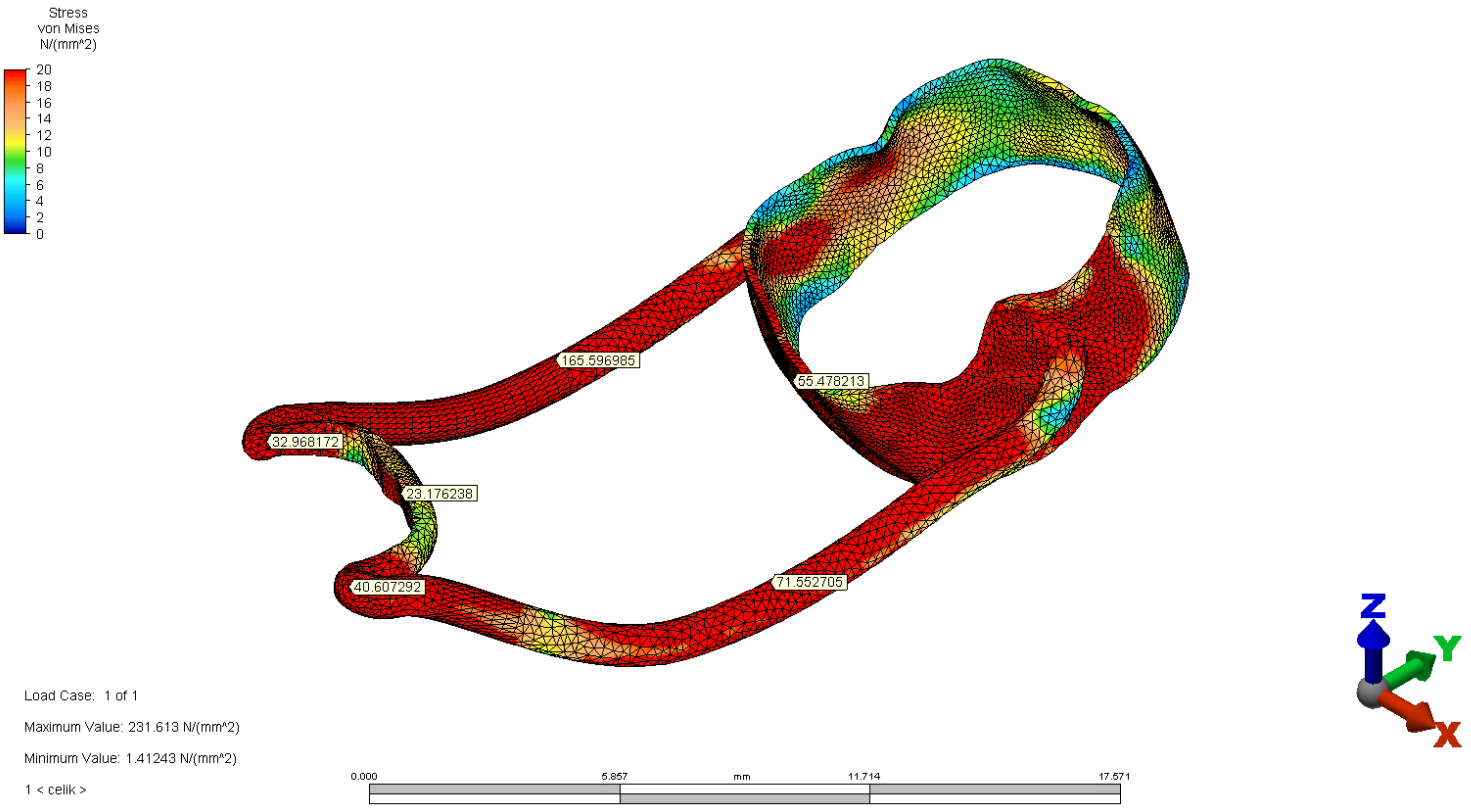

FIGURE 11. FSM with curved and surround arms. The von Mises Stress Scale in Test Model 4 is shown using a stress scale and spatial coordinates.

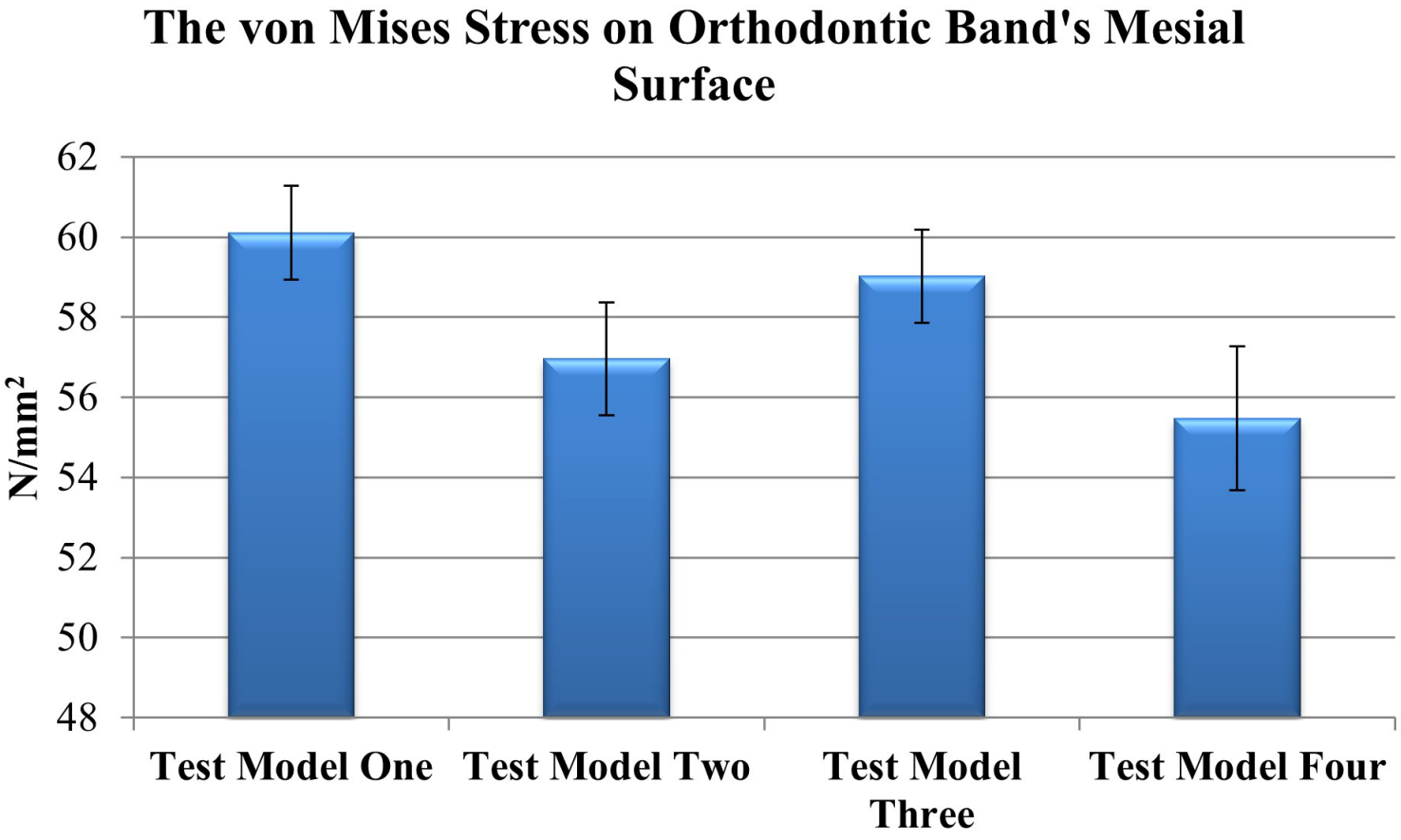

FIGURE 12. The von Mises Stresses on the mesial surface of the orthodontic band.

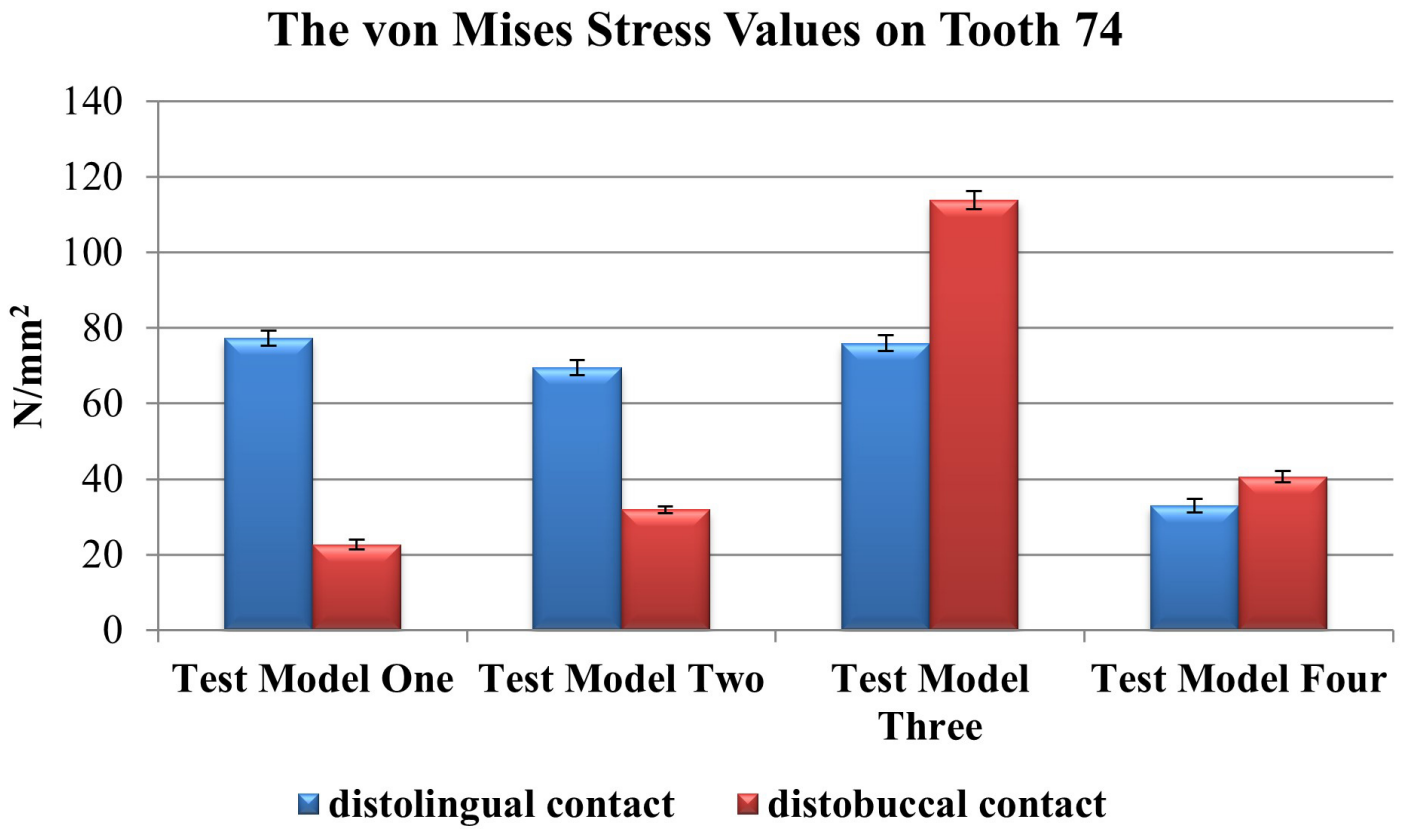

FIGURE 13. The von Mises Stress values on tooth 74's distal contact points for all test models.

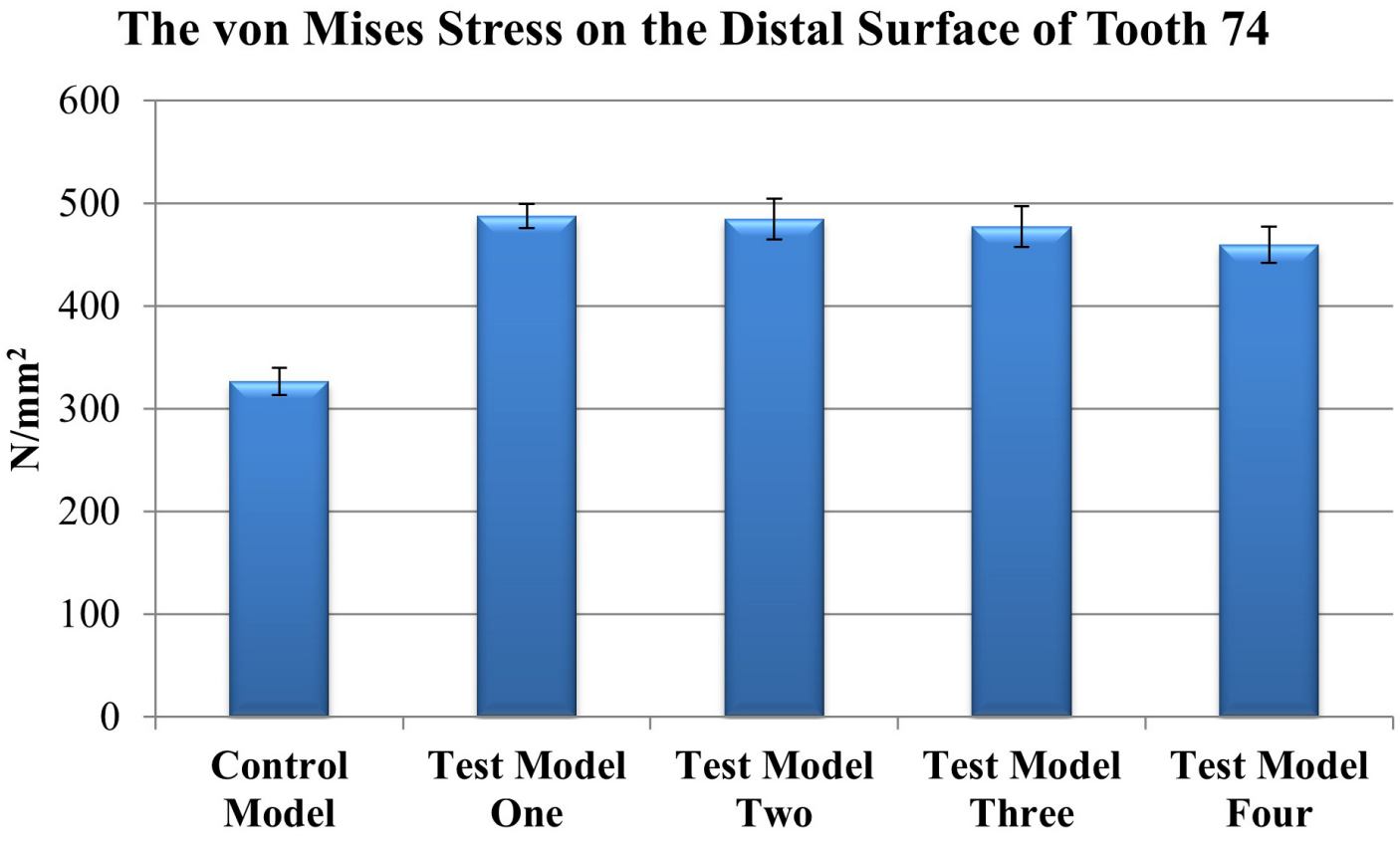

FIGURE 14. The von Mises Stress values on tooth 74's distal surface for all test models.

groups ($p < 0.001$), and multiple comparisons and test models also indicated significant differences ($p < 0.001$) in this regard.

The cortical and cancellous bone results were also evaluated. The variations among the five groups were found to be significantly different for the cortical bone ($p < 0.001$). Significant differences were also found in multiple comparisons and test models ($p < 0.001$, respectively). However, no significant difference was observed between the five groups in cancellous bone ($p = 0.194$). The maximum principal stresses were found to accumulate at the base of the alveolar socket of the mesial root of tooth 36, while the minimum principal stresses were identified at the mesio-marginal area of the alveolar crest in the mesial wall. These results indicate that compressive stresses accumulated at the mesial base of the alveolar socket, while tensile stresses accumulated on the mesial-marginal alveolar bone ridge (Fig. 15).

4. Discussion

In this present study, stress accumulation on FSMs and the effect of their arm design were investigated using FEA for the first time. To ensure that our study results closely resemble clinical conditions, we utilized CBCT images of a patient who had undergone premature extraction of the primary mandibular second molar tooth. These images were processed, and the stress values accumulated on four FSMs with different arm designs were analyzed. Additionally, we evaluated the potential reasons for FSM failure by considering the differences in arm design.

The sequelae of not placing an FSM following premature tooth extraction can lead to various consequences, including arch length reduction, crowding, midline discrepancy, ectopic eruptions, dental impactions, the formation of periodontal pockets due to mesial tipping, and over-eruption of the opposing teeth [22]. Further, complications that may arise after FSM placement include gingivitis, the formation of gingival pockets, the development of caries, FSM decementation, and embedding of the FSM into the gingiva [23]. Previous studies on the failure of FSMs mainly focused on bonding and cementation failures [3, 10], and upon reviewing related literature, we found a lack of research regarding FSM design and its effect on decementation failure.

The hypothesis of this study was rejected based on the results obtained. Test Model One exhibited the highest von Mises stress on the buccal arm, followed by Test Model Four on the lingual arm, highlighting the significance of utilizing CBCT scans in this study. Notably, this study identified, for the first time, a correlation between decementation failure and the mesial surface of the orthodontic band. This can be attributed to two potential factors: firstly, the mesial position of the permanent mandibular first molar tooth, and secondly, the transmission of accumulated stress in the SM arms to the mesial aspect of the orthodontic band.

However, it is important to note that there were variations in the accumulation of von Mises stress in the arms, with a more significant accumulation of stress observed in the lingual arms compared to the buccal arms in all study groups.

The von Mises stress values observed in the arms were inversely proportional to those on the buccal and lingual aspects of the bands. In other words, increased stress accumulation in the arms correlated with decreased stress values in the bands, suggesting that when more force is directed towards the tooth

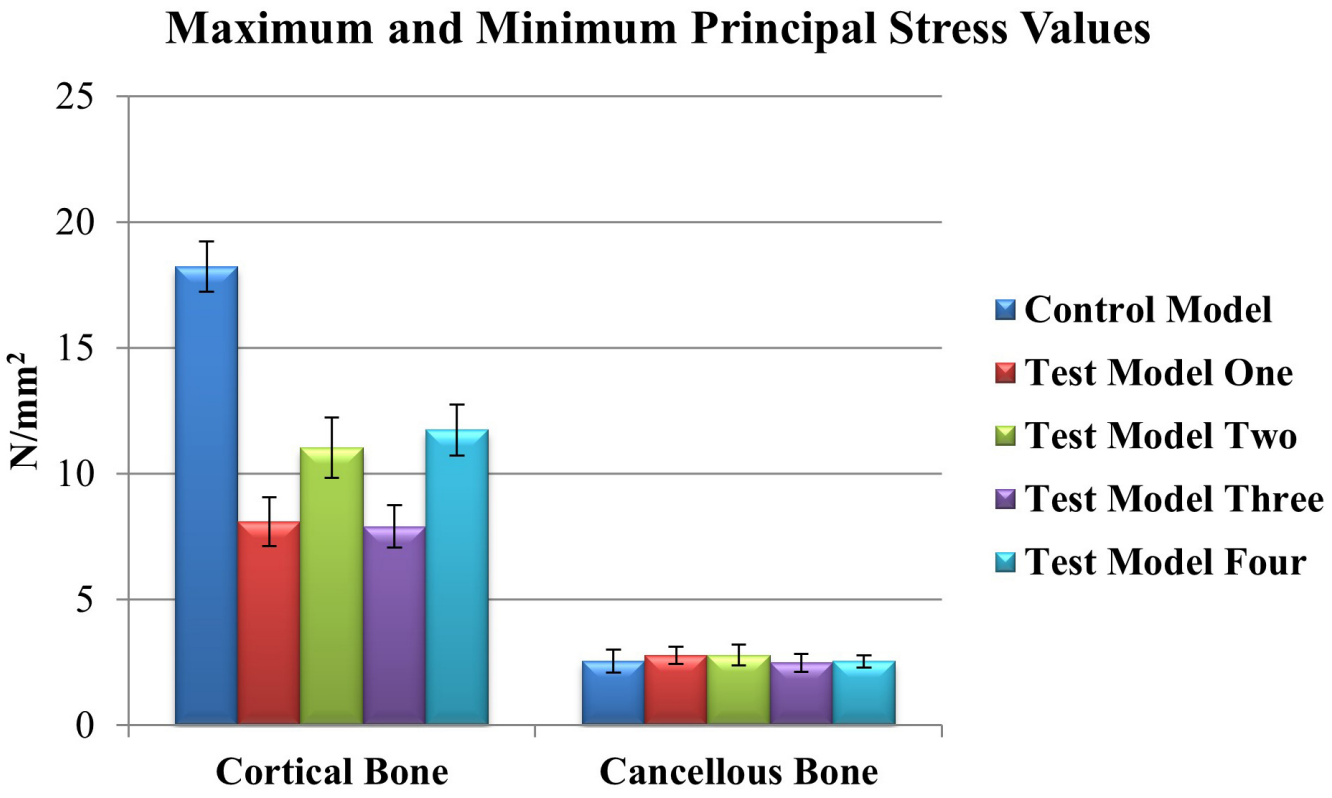

FIGURE 15. Maximum and minimum principal stress values on the root dentin surfaces for all models.

located mesial to the edentulous region, the stress values on the band consequently decrease.

Moreover, Fig. 15 shows a two-fold increase in both compressive and tensile forces in cortical and cancellous bones with SM cementation across all tested groups compared to the control model. This increase is likely due to the SM functioning as a force-transmitting element within the established fixed mechanical system. Notably, we observed a significant accumulation of tensile forces at the mesial-marginal border of the alveolar bone. The rise in tensile stress in this area when teeth are mesialised is linked to bone loss at the mesial-marginal border of the alveolar bone, which is evident in both pediatric and adult patients who have been edentulous for a long time [22].

The mesial tooth gripping effect of the FSM arm design plays a crucial role in transmitting the chewing force to the mesial tooth over a wider surface, and it is important to note that previous studies have highlighted the potential for caries formation with FSMs [23, 24]. Therefore, it is recommended that patients and parents be informed about the potential caries-forming effect associated with the arm design when it surrounds the mesial tooth.

Proximal caries are the most common cause of premature tooth loss in pediatric patients [25]. Although we simulated the intraoral condition of a child with early tooth loss in this present study, in a clinical setting, it should be considered that the primary mandibular first molar tooth (tooth 74) is likely to be restored due to proximal caries or decay of tooth 75. In our simulation model, tooth 74 underwent pulpotomy and was restored with a stainless-steel crown. Thus, in future studies, evaluating the stress accumulation caused by the FSM on the tooth located mesial to the edentulous space could provide more insights regarding such issue. Notably, the significant difference observed between the groups in terms of the von Mises stresses on tooth 74 (Fig. 13) highlights the need for further investigation and understanding of the stress distribution and its impact on restored teeth in the presence of FSMs.

FEA is an engineering software program that allows detailed investigation of tensile and compressive stresses and displacements in structures with complex geometry through mathematical calculations [26]. The method allows for detailed investigations and modeling of structures to closely resemble the original design, enabling the calculation of stress values that reflect the physical properties of the models realistically [27]. In addition, to ensure that the models simulate the clinical condition as closely as possible, it is essential to determine boundary conditions correctly [13].

Various stress formulas are utilized in dental FEA studies, including principal and von Mises stresses [28]. Principal stresses can be calculated individually in different global coordinate directions (x, y, z) as minimum, intermediate, and maximum values. In contrast, von Mises stresses are calculated by combining different principal stresses [11]. The von Mises stress analyses were recorded for ductile materials (*i.e.*, steel, alloy and implant materials), while the principal stress analyses were performed for brittle materials (*i.e.*, cortical and cancellous bone). This study focused on the von Mises stress criterion, considering the differences in tensile and compressive strengths. Biological dental structures tend to be more resistant to compressive stresses than tensile stresses, suggesting that tensile stresses are more likely to cause greater damage [12]. Irrespective of the number of tests (*i.e.*, collision and impact or stress resistance) repeated, the same precise mathematical results are obtained using the FEA method, indicating that there was no need to use traditional statistical analyses in studies conducted using the FEA method. Therefore, our presented results can be interpreted visually and based on numerical values [11].

The results of this present study suggest the need to make FSMs using more flexible, durable and cement-bonded materials, thereby requiring the need for materials that can be processed up to the thickness of orthodontic bands using advanced technology and designed as an arm and band produced in one piece. In this regard, previous studies have explored the use of polyetheretherketone (PEEK) material in producing lingual holding arches and removable SMs [29, 30]. In a case report, researchers successfully monitored a patient with an SM made of PEEK material for nine months [30]. However, it was understood that the aesthetic properties of PEEK material should also be improved [29, 30].

This study has several limitations that should be acknowledged. First, the simulations were performed on a pediatric dental model obtained from the CBCT database. However, it was observed that tooth 36 in the study model was mesialized due to tipping. To achieve results closer to those observed in clinical conditions, the study was designed from an ethical perspective such that no other patient would receive radiation. However, it is important to recognize that simulating chewing forces on a non-mesialized tooth may yield different results, warranting further investigation. Another limitation is that the study did not evaluate the stress accumulation resulting from the chewing force transmitted to tooth 74 and its potential consequences.

5. Conclusions

FSMs play a crucial role in preventing space loss after early primary tooth extraction. However, the impact of FSM arm design has been revealed for the first time in this study. Based on the results obtained, a curved arm design of the FSM effectively transfers the chewing force towards the mesial region by encompassing the distal surface of the adjacent tooth in the edentulous area. Increasing the arm length of the FSM following the loss of a single tooth leads to a decrease in stress accumulation on the orthodontic band. Thus, the arms should be curved and wrapped around the tooth in contact with the mesial area at an optimum level. Additionally, surrounding the orthodontic bands by increasing the soldered area of the arms can help prevent excessive stress accumulation on the FSM mechanics, reducing the likelihood of orthodontic band decementation or arm solder breakage. Notably, no other study has examined FSMs using FEA methods together. Therefore, further studies are warranted to explore the use of more flexible and force-absorbing materials in FSMs.

In conclusion, while FSMs are commonly used to prevent space loss, the influence of arm designs has not been previously considered as a factor contributing to FSM failure. Increasing

the arm length of the FSM after the loss of a single tooth can decrease stress accumulation on the orthodontic band.

To optimize the design, curved arms that wrap around the tooth in contact with the mesial area should be employed. Moreover, enhancing the soldered area where the arms connect to the orthodontic bands can be beneficial. Further research is needed to explore the use of more flexible and force-absorbing materials in FSMs.

AVAILABILITY OF DATA AND MATERIALS

The datasets used and/or analyzed during the current study are available from the corresponding author on reasonable request.

AUTHOR CONTRIBUTIONS

ÖD—planned this study and carried out the writing of the manuscript. SSAD—checked the study simulations models design and their accuracy according to anatomical structures. ÖD and SSAD—interpreted the obtained finite element results and approved the manuscript.

ETHICS APPROVAL AND CONSENT TO PARTICIPATE

The FE models used in this study were acquired after the Clinical Research Ethics Committee of the Medical School of Afyonkarahisar approved the study (2019/68). The written consent form was obtained from child and her parents.

ACKNOWLEDGMENT

The authors would like to thank “Ay Design and Tinus Technologies” companies for their technical contributions to this study.

FUNDING

This study was funded by Afyonkarahisar Health Science University Scientific Research Projects Coordinatorship. Projects Number: 19.DİŞ.005.

CONFLICT OF INTEREST

The authors declare no conflict of interest.

REFERENCES

[1] Law CS. Management of premature primary tooth loss in the child patient. Journal of the California Dental Association. 2013; 41: 612–618.

[2] Nascimento EB, Rodrigues R, Manso MC. Prevalence of dental floss use in deciduous dentition: a systematic review and meta-analysis. International Journal of Dental Hygiene. 2023; 21: 116–127.

[3] Watt E, Ahmad A, Adamji R, Katsimbali A, Ashley P, Noar J. Space maintainers in the primary and mixed dentition—a clinical guide. British Dental Journal. 2018; 225: 293–298.

[4] Barros SE, Siqueira SP, Janson G, Chiqueto K. Short-term efficacy of vacuum-formed maintainer for deciduous second molar space maintenance in the mixed dentition: a single-centre, randomized controlled clinical trial. Orthodontics & Craniofacial Research. 2021; 24: 502–510.

[5] Heidari A, Mokhtari S, Hamrah MH, Tavana Z, Heydarigoojani M, Tavana N. Investigating the factors affecting the need for unilateral space maintainer for first primary molars in late mixed dentition. BioMed Research International. 2022; 2022: 7604144.

[6] Lee J. Fully digital workflow for the fabrication of a tooth-colored space maintainer for a young patient. Journal of Esthetic and Restorative Dentistry. 2023; 35: 561–566.

[7] Tribst JPM, Dal Piva AMDO, Bottino MA, Kleverlaan CJ, Koolstra JH. Mouthguard use and TMJ injury prevention with different occlusions: a three-dimensional finite element analysis. Dental Traumatology. 2020; 36: 662–669.

[8] Bragança GFD, Vilela ABF, Soares PBF, Tantbirojn D, Versluis A, Soares CJ. Influence of ceramic veneer thickness and antagonist on impact stresses during dental trauma with and without a mouthguard assessed with finite element analysis. Dental Traumatology. 2021; 37: 215–222.

[9] Qudeimat MA, Sasa IS. Clinical success and longevity of band and loop compared to crown and loop space maintainers. European Archives of Paediatric Dentistry. 2015; 16: 391–396.

[10] Khanna S, Rao D, Panwar S, Pawar BA, Ameen S. 3D printed band and loop space maintainer: a digital game changer in preventive orthodontics. Journal of Clinical Pediatric Dentistry. 2021; 45: 147–151.

[11] Demirel A, Bezgin T, Sarı Ş. Effects of root maturation and thickness variation in coronal mineral trioxide aggregate plugs under traumatic load on stress distribution in regenerative endodontic procedures: a 3-dimensional finite element analysis study. Journal of Endodontics. 2021; 47: 492–499.e4.

[12] Demirel A, Sarı Ş. Are increased masticatory forces risk for primary 2nd molars without successors? A 3D FEA study. Journal of Clinical Pediatric Dentistry. 2019; 43: 64–68.

[13] Firmiano TC, de Oliveira AA, Costa PVDM, Cardoso LS, Pereira RD, Veríssimo C. Influence of different ethylene-vinyl acetate brands used for custom-fitted mouthguard fabrication on the stress and strain during an impact. Dental Traumatology. 2022; 38: 431–438.

[14] Belli S, Eraslan O, Eskitascioglu G. Effect of root filling on stress distribution in premolars with endodontic-lesion: a finite elemantal analysis study. Journal of Endodontics 2016; 42: 150–155.

[15] Jang Y, Hong HT, Roh BD, Chun HJ. Influence of apical root resection on the biomechanical response of a single-rooted tooth: a 3-dimensional finite element analysis. Journal of Endodontics. 2014; 40: 1489–1493.

[16] Matsuyama Y, Motoyoshi M, Tsurumachi N, Shimize N. Effect of palate depth, modified arm shape, and anchor screw on rapid maxillary expansion: a finite element analysis. European Journal of Orthodontics. 2015; 37: 188–193.

[17] Romeed S, Dunne S. Stress analysis of different post-luting system: a three-dimensional finite element analysis. Australian Dental Journal 2013; 58: 82–88.

[18] Lee H, Jo M, Sailer I, Noh G. Effects of implant diameter, implant-abutment connection type, and bone density on the biomechanical stability of implant components and bone: a finite element analysis study. The Journal of Prosthetic Dentistry. 2022; 128: 716–728.

[19] Karimizadeh Z, Kamali Sabeti A, Rafatjou R. Maximum equivalent stress induced and the displacement of the developing permanent first molars after the premature loss of primary second molars: a finite element analysis. Dental and Medical Problems. 2020; 57: 401–409.

[20] Hollanders ACC, Kuper NK, Huysmans MCDNJM, Versluis A. The effect of occlusal loading on cervical gap deformation: a 3D finite element analysis. Dental Materials. 2020; 36: 681–686.

[21] Owais AI, Shaweesh M, Abu Alhaija ESJ. Maximum occusal bite force for children in different dentition stages. The European Journal of Orthodontics. 2013; 35: 427–433.

[22] Köseoğlu S, Fidancıoğlu A, Sağlam M, Savran L. Management of a periodontal pocket using a removable orthodontic appliance and nonsurgical periodontal therapy. Case Reports in Dentistry. 2015; 2015: 374850.

[23] Gurcan AT, Koruyucu M, Kuru S, Sepet E, Seymen F. Effects of fixed and removable space maintainers on dental plaque and DMFT/dft values. Odovtos International Journal of Dental Sciences. 2021; 23: 137–147.

[24] Martín-Vacas A, Caleya AM, Gallardo NE. Comparative analysis of space maintenance using transpalatal arch and nance button. Journal of Clinical Pediatric Dentistry. 2021; 45: 129–134.

[25] Ortiz MIG, Ribeiro MES, Lima DANL, Silva CM, Loretto SC, da Silva e Souza Júnior MH. Compliance of randomized clinical trials on dental caries prevention methods with the consort statement: a systematic review. Journal of Evidence Based Dental Practice. 2021; 21: 101542.

[26] Carvalho V, Soares P, Verissimo C, Pessoa R, Versluis A, Soares C. Mouthguard biomechanics for protecting dental implants from impact: experimental and finite element impact analysis. The International Journal of Oral & Maxillofacial Implants. 2018; 33: 335–343.

[27] Firmiano TC, Oliveira MTF, de Souza JB, Soares CJ, Versluis A, Veríssimo C. Influence of impacted canines on the stress distribution during dental trauma with and without a mouthguard. Dental Traumatology. 2019; 35: 276–284.

[28] Alper B, Gultekin P, Yalci S. Application of finite element analysis in implant dentistry. 10th edn. InTech: London. 2012.

[29] Guo H, Wang Y, Zhao Y, Liu H. Computer-aided design of polyetheretherketone for application to removable pediatric space maintainers. BMC Oral Health. 2020; 20: 201.

[30] Ierardo G, Luzzi V, Lesti M, Vozza I, Brugnoletti O, Polimeni A, *et al*. Peek polymer in orthodontics: a pilot study on children. Journal of Clinical and Experimental Dentistry. 2017; 9: e1271–e1275.

How to cite this article: Özgür Doğan, Suat Serhan Altıntepe Doğan. Arm design of band and loop space maintainer affects its longevity: a patient-specific finite element study. Journal of Clinical Pediatric Dentistry. 2024; 48(1): 171-183. doi: 10.22514/jocpd.2024.019.